Power Electronic Systems
Laboratory

Proceedings of the International Power Electronics Conference - ECCE Asia (IPEC 2014), Hiroshima, Japan, May 18-21, 2014

Concept and Experimental Evaluation of a Novel DC - 100 MHz Wireless Oscilloscope

Y. Lobsiger,
G. Ortiz,
D. Bortis,
J. W. Kolar

Eidgenössische Technische Hochschule Zürich
Swiss Federal Institute of Technology Zurich

Concept and Experimental Evaluation of a Novel DC – 100 MHz Wireless Oscilloscope

Yanick Lobsiger*†, Gabriel Ortiz*†, Dominik Bortis*†, and Johann W. Kolar*

*ETH Zurich
Power Electronic Systems Laboratory
Physikstrasse 3, 8092 Zurich, Switzerland
lobsiger@lem.ee.ethz.ch

†Enertronics GmbH
c/o ETH Zurich, Power Electronic Systems Lab.
Physikstrasse 3, 8092 Zurich, Switzerland
info@enertronics.ch

***Abstract*—A wireless oscilloscope featuring 100 MHz analog bandwidth and ultra-high isolated measurement channels is presented in this paper. In order to visualize the benefits of this potential-free measurement system, the paper starts with a revision of commonly utilized isolated voltage and current measurement concepts. With a clear understanding of the benefits given by a high-bandwidth, high-isolated and highly common mode immune measurement system laid down, the details about the wireless oscilloscope and its potential-free input channels are presented. Experimental measurements comparing the state of the art isolated voltage and current measurement concepts with the proposed wireless oscilloscope regarding common mode rejection ratio and signal-to-noise ratio are presented, showing the excellent performance of the introduced measurement system.**

I. Introduction

During the experimental testing of power electronic circuits, accurate measurement of the converter's voltages and currents is required in order to ensure the correct operation of the system. Moreover, very often these currents and voltages are referred to individual floating potentials, thus the measurement principle must provide a minimum isolation level in order to be safely coupled to the system.

As an example, Fig. 2 (a) shows a state of the art solution for an electric drive system. Here, a cascaded, i.e. series, arrangement of N cells allows the connection of the drive system directly to Medium Voltage (MV), whereby the isolation and voltage adaptation is performed by a high-power DC-DC converter. The outputs of these DC-DC converters are connected in parallel in order to supply the inverter driving the electrical machine.

A detailed internal representation of one converter cell is shown in Fig. 2 (b). This cell consists of an input H-bridge responsible for the rectification of the input voltage while performing power factor correction. At the input of this rectifier, typically a 50 Hz input current with superimposed high-frequency ripple is found along with the cells' switched voltage waveform. It should be noted that, due to the series connection at the input, these voltages and currents are not referred to ground but rather to floating and fast changing potentials. Moreover, within the converter's cell, the DC-DC converter is characterized by an operation at medium-frequency level, whereby fast dynamic behavior of the transformer voltages and currents are expected. Additionally, often a switching performance assessment, involving simultaneous measurement of its emitter current, collector-emitter and gate voltages is desired in order to ensure the safe operation of the semiconductor device. In this case, fast transients are to be expected during the switching process, thus a high-bandwidth, isolated and highly common mode immune measurement concept is required.

This paper provides a revision of the state of the art isolated voltage and current measurement concepts in Section II, whereby the main limitations of these concepts will be highlighted. With the desired features of the new measurement concept outlined, the details of the proposed wireless oscilloscope depicted in Fig. 1 will be shown in Section III. The performance of the proposed oscilloscope in comparison to state of the art voltage and current measurement concepts under typical testing conditions (floating potentials, fast transients and low voltage signals, among others) is presented. The paper finalizes with a summary and outlook of further improvements and extensions of the wireless scope in Section V.

Fig. 1: Enertronics' wireless oscilloscope channel, featuring 100 MHz analog bandwidth, 400 MS/s sampling rate, no intrinsic limit on isolation and high common mode immunity.

II. State of the Art Measurement Concepts

In order to identify the main limitations of today's isolated measurement principles for voltage and current in power electronic systems, a review of these concepts will be presented in the following sections.

A. Isolated Voltage Measurement

The main utilized isolated measurement concepts are *1) Differential Probes*, and *2) Optic-based Concepts*, whereby the details about their operation are presented in the following.

1) Differential Probes: Differential measurement of voltages is the most common method for safely measuring high voltages which are not referred to the scope's ground potential. These differential probes typically feature an high-ohmic input voltage divider followed by an instrumentation amplifier, as shown in Fig. 3 (a). By appropriately selecting the resistors in this circuit, the output voltage v_{M} of the probe can be described by

$$v_{\mathrm{M}} = v_{\mathrm{IN}} \cdot A_{\mathrm{DM}} + v_{\mathrm{CM}} \cdot A_{\mathrm{CM}}, \tag{1}$$

where v_{IN} is the input voltage to be measured, v_{CM} is the common mode voltage referred to the scope's ground potential, A_{DM} is the probe's differential mode gain and A_{CM} is the probe's common mode

978-1-4799-2705-0/14/$31.00 ©2014 IEEE

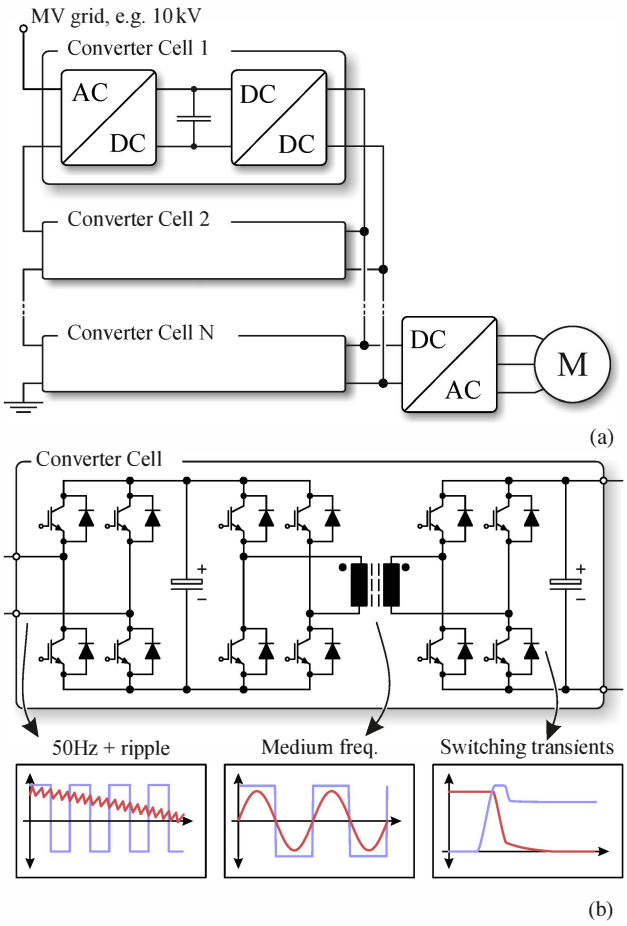

Fig. 2: Typical power electronic system to be measured by isolated voltage and current probes. In (a), a cascaded connection of cells supplying ultimately a machine is presented. These cells, whose detailed view is shown in (b), are characterized by a floating potential given by the aforementioned series connection at the input side.

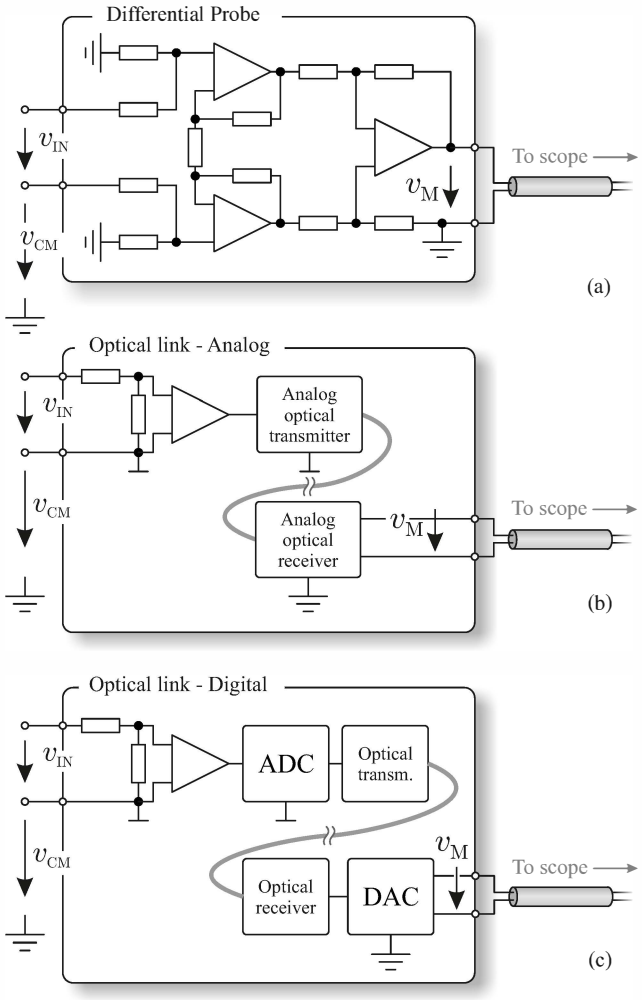

Fig. 3: Isolated voltage measurement concepts: (a) Differential probe based on an input instrumentation amplifier; (b) Analog optical link, the analog signal is modulated and transmitted through an fiber-glass optic link; (c) Digital optical link, the analog signal is converter to digital at the probe side and transmitted via fibre optic to the receiver side where its reconverted to analog.

attenuation. Ideally this common mode attenuation A_{CM} is close to zero, achieving the ideal relation between input and output voltage

$$v_M \approx v_{IN} \cdot A_{DM}. \quad (2)$$

In practice however, due to component tolerances and differences in the AC-characteristics of the probe's inputs, the value of A_{CM} is not zero and deteriorates with increasing frequency, thus a comparably low Common Mode Rejection Ratio (CMRR) is achieved. This introduces errors in the measurement due to a strong presence of common mode voltage components in the output signal v_M. In addition, due to the high input voltage divider, the differential probe suffers from a low Signal-to-Noise Ratio (SNR).

2) Optical-Based Concepts: In order to overcome the limitations concerning SNR, CMRR and input voltage range, isolated measurement systems can be used. In the following, different concepts providing a galvanic isolation between a floating reference voltage and earth ground are presented.

The simplest way to decouple the measurement system from any ground potential is to use a battery powered measurement system, which consequently features an unlimited voltage isolation [1–3]. In addition, the coupling capacitance between the measurement system connected to the floating circuitry and ground is small, thus, the capacitive current caused by common mode voltage transients and the influence of the measurement system on the current or voltage waveforms can be minimized.

Unlimited voltage isolation of the signal path can be achieved e.g. by means of an analog optical link where the light intensity is modulated as a function of the input signal's amplitude as shown in Fig. 3 (b) and presented in [1]. The major disadvantage of an analog optical transmission systems is the ageing of the optical transmitter and receiver units, which have to be re-calibrated periodically.

If the optical signal transmission is performed digitally as shown by the scheme presented in Fig. 3 (c), these ageing effects are negligible. Then, for the optical link, which is used as a real-time signal isolator of a digital channel, a data transfer rate of several Gigabit per second is needed in order to achieve a reasonable analog bandwidth of around 100 MHz. Even if such fast optical links are commercially available, these transmitters are not suitable for battery powered systems due to their high power consumption - typically in the range of one Watt - which leads either to a reduced battery runtime or a larger measurement system with higher battery storage capacity.

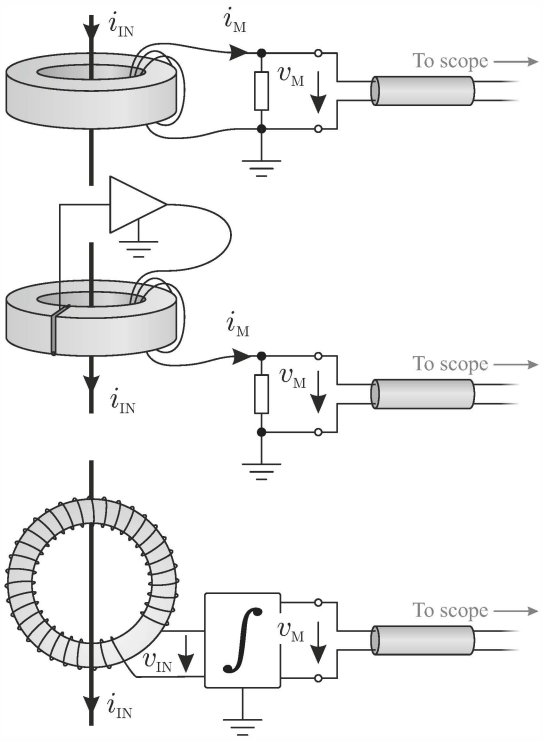

Fig. 4: Isolated current measurement principles: (a) Current transformer with burden resistor; (b) Compensated current transformer for measurement of DC and AC signals; (c) Rogowski coil and its respective integration block.

Furthermore, depending on the measurement system's housing, a higher power consumption could also result in possible overheating of the measurement system. On the other hand, however, if the housing of the measurement system is enlarged, the coupling capacitance of the measurement system to ground is also increased, thus, degrading the measurement quality.

B. Isolated Current Measurements

In case of isolated current measurement principles, the main utilized concepts in power electronics are *1) Current transformer, 2) Compensated Current Transformer* and *3) Rogowski Coil*, all of which are presented in Fig. 4 and will be described in the following.

1) Current Transformer: A current transformer consists of a magnetic core with a secondary winding and a burden resistor. The current to be measured i_{IN} flows through the core's window enabling a magnetic coupling of the input current i_{IN} and the output current i_{M}. The burden resistor R_{B} is then responsible for translating this measured current i_{M} into a voltage signal v_{M} to be captured by the scope. This way, the relation between input current i_{IN} and the measured voltage v_{M} is:

$$v_{\mathrm{M}} = R_{\mathrm{B}} \frac{i_{\mathrm{IN}}}{N_{\mathrm{CT}}}, \tag{3}$$

where N_{CT} is the number of secondary turns if the current transformer.

However, the expression in (3) is only valid as long as a good coupling between primary and secondary can be ensured, which is not the case at low frequencies [4]. As a consequence, current transformers feature a high-pass characteristic and are therefore not suitable for measurement of DC and / or low frequency signals.

Furthermore, the upper corner frequency of the current transformer, defining the bandwidth of the sensor, is related to the leakage inductance of the transformer, which is typically kept as low as possible by minimizing the size of the sensor. Reducing the size of the sensor, however, deteriorates its isolation performance given the comparatively small distances available for introduction of isolation layers. The result is a clear trade-off between the bandwidth and isolation level of the current sensor.

2) Compensated Current Transformer: As mentioned earlier, a current transformer is not able to measure currents in the low frequency range. In order to overcome this fundamental limitation, a magnetic flux sensing device can be inserted in the air-gap of the core as depicted in Fig. 4 (b). The signal from this sensor is utilized in a closed loop arrangement in order to compensate the low frequency components of the measured current and therefore extending the operation range of the sensor to the low frequency (including DC) range [5], thus enabling measurement of current components from DC to the high MHz range.

The key component in this compensated current sensor arrangement is the flux sensor which is most commonly a semi-conductive Hall-element [6], or a flux-gate-based sensor [7]. The implementation of these flux sensors involves advanced manufacturing techniques and compensation circuits within the sensor. In addition, since the current transformer is still responsible for the measurement of the high-frequency spectra of the current, the same trade-off between isolation and bandwidth is found as in an uncompensated current transformer.

3) Rogowski Coil: A very common current measurement concept in power electronics is the Rogowski coil. This sensor is based on inductive coupling of the input current i_{IN} and an air coil surrounding this conductor as shown in Fig. 4 (c). This inductive coupling results in an coil output voltage which is proportional to the derivative of the input current i_{IN}. It is therefore necessary to integrate this signal in order to obtain a voltage signal v_{M} proportional to the input current i_{IN},

$$v_{\mathrm{M}} = \int v_{\mathrm{IN}} dt = M \int \frac{di_{\mathrm{IN}}}{dt} dt, \tag{4}$$

where M represents the coupling inductance between the input conductor and the Rogowski coil. As can be seen, an integration is required in order to reconstruct the input current's waveform. This integration process represents the main challenge in the implementation of Rogowski-coil-based current probes, as problems associated with drifting due to DC biases are very often encountered. This drifting problems are counteracted with circuits featuring a high-pass characteristic in the low frequency range of the integration circuit, thus no DC signals can be measured [8].

In addition, as well as with the current transformers, the dimensions of the coil itself are directly related to the bandwidth of the sensor, resulting in a tight coupling between isolation and bandwidth.

C. Summary of State of the Art Isolated Measurement Concepts

Isolated voltage and current sensor manufacturers offer solutions with one of the previously described principles featuring different bandwidths and isolation levels. These solutions are conveniently summarized in a bandwidth vs. isolation map in Fig. 5. In case of the voltage sensors, manufacturers [9–13] were selected for the differential probe measurements while [14, 15] were considered for the optically isolated measurement concept. In case of current measurement principles, [9, 10] represent the compensated current transformer concepts while [16] and [13] were selected for the

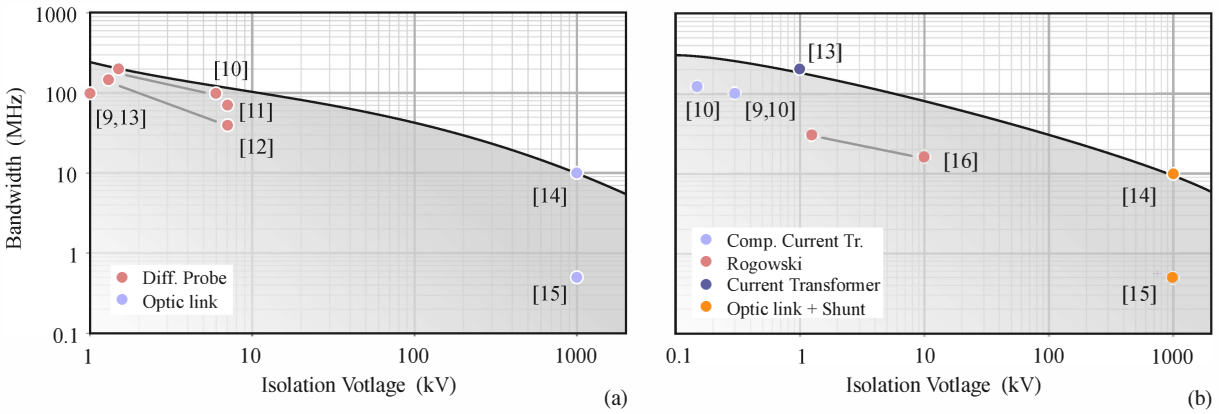

Fig. 5: Summary of state-of-the-art isolated voltage and current measurement concepts displayed in a bandwidth vs. isolation voltage for (a) voltage sensors and (b) current sensors.

Rogowski and current transformer principles respectively. In addition, a optically isolated measurement as the ones described in the voltage measurement principles are considered since a non-isolated current transducer, e.g. a shunt resistor, can be attached at its input, thus enabling isolated current measurement.

From Fig. 5 the aforementioned trade-off between bandwidth and isolation in voltage and current sensing principles can be confirmed by manufacturer-provided data. In the voltage map (cf. Fig. 5 (a)) the highest bandwidth sensor is fabricated by [10] with a maximum specified isolation of 1.5 kV whereas the highest isolation solution is represented by [14] with a bandwidth of 10 MHz. In case of the current map shown in Fig. 5 (b) the highest bandwidth is achieved by the current transformer from [13] with a maximum isolation voltage of 1 kV and the maximum isolation voltage is provided by the coupled non-isolated current measurement with the optic-based solutions, as mentioned earlier.

The bandwidth and isolation limitations represented in Fig. 5 can be overcome by a new concept in oscilloscope data acquisition: If the isolation is provided by each channel of the oscilloscope, the voltage / current probe can be optimized for maximum bandwidth and minimum isolation, thus reaching an unprecedented performance in isolated measurement systems. This is main principle of the wireless voltage probe proposed in this paper, whereby its implementation details and the means to achieve a high bandwidth / sampling rate are detailed in the next section.

III. Wireless Oscilloscope

In contrast to the state of the art isolated voltage and current probes detailed in the last section, a combined high voltage and high bandwidth isolation of an oscilloscope's input channel can be achieved, if the isolation is not provided to the real-time signal / data stream but only to that data, which is recorded / stored by the scope. In this way, the bandwidth requirement on the isolated channel is significantly lower and can be achieved by a digital optical or even a wireless data transmission. This concept is followed by the proposed wireless oscilloscope, which is described in the following.

A schematic overview of the wireless oscilloscope is depicted in Fig. 6. It consists of multiple isolated input channels and a graphical user interface, which exchange the configuration parameters and the measurement data wireless. The battery powered operation of the channels enables a autonomous and fully isolated operation of the system.

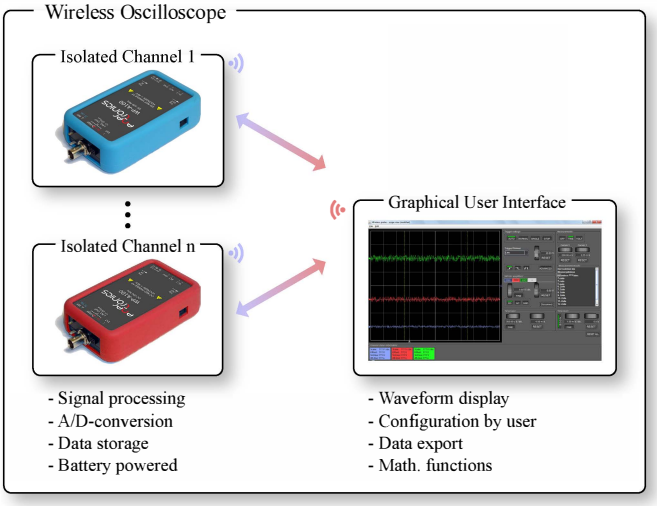

Fig. 6: Schematic overview of the wireless oscilloscope consisting of multiple isolated input channels and a graphical user interface (GUI) running on a computer. The wireless communication between the channels and the GUI is based on the Bluetooth technology.

A. Hardware and Software Implementation

In order to demonstrate the feasibility and finally also to proof the performance of the wireless scope, a hardware prototype has been built and a GUI prototype has been programmed. In the following, these prototypes will be explained in more detail.

1) Isolated Input Channel: The hardware part of the wireless oscilloscope, i.e. an isolated measurement channel, has been implemented in a compact enclosure with silicone cover as shown in Fig. 7. It features a BNC connector for the measurement signal input, as it is the case for a conventional oscilloscope, enabling the use of any kind of external sensor with BNC output. An external passive probe can be connected and calibrated by means of the calibration signal output. If multiple channels are used simultaneously, the internal synchronization platform performs a high accuracy wireless synchronization of typ. ±10 ns in between all probes. This synchronization error can ca. be halved, if the channels are connected among each other using the optical trigger in- and outputs. The internal Li-Ion batteries are charged by means of an external DC power supply. An overview of the internal setup of an input channel is depicted in Fig. 8 and the

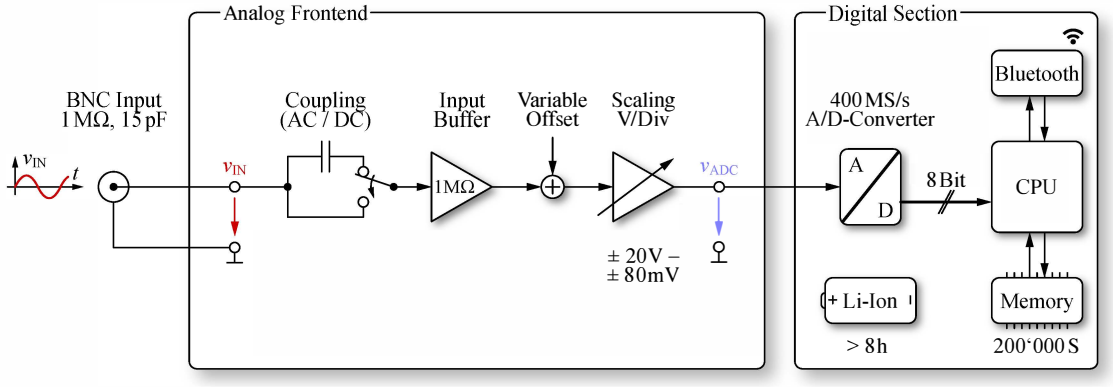

Fig. 8: Schematic overview of an input channel's internal setup.

Fig. 7: Prototype of the wireless oscilloscope with physical dimensions of $141\,\text{mm} \times 81\,\text{mm} \times 32\,\text{mm}$. Front side: (1) BNC connector for the input signal, (2) calibration signal output and (3) interface for external sensors; back side: (4) I/O power switch, (5) status and charge indication LEDs and (6) connector for the battery charger; left / right side: (7) optical trigger out- and (8) inputs.

scope's corresponding specifications are listed in Table I.

2) Graphical User Interface (GUI): The counterpart to the isolated channels is the GUI which is similar to the mechanical knobs and the screen of a conventional oscilloscope, where the waveforms of all channels are displayed and where the user can make the configuration for all channels of the wireless oscilloscope. A screen shot of the implemented GUI is depicted in Fig. 9. Contrary to a conventional oscilloscope, where typically only four analog channels can be used, the GUI theoretically enables to connect an unlimited amount of fully isolated input channels. On the left hand side, the waveforms and the corresponding settings of all channels are displayed. On the right hand side, the user can configure the trigger, the individual vertical and horizontal settings of all channels, the cursors and the zoom-function. The GUI also allows to export and import measurement data and settings.

TABLE I: Specification overview of the wireless oscilloscope prototype.

Analog Bandwidth	DC – 100 MHz
Sampling Rate (max.)	400 MS/s
Memory Depth (max.)	200 kS
Resolution	8 Bit
Input Voltage Range	±80 mV . . . ± 20 V ±800 mV . . . ± 200 V (10:1 passive probe) . . .
Input Impedance	1 MΩ, 15 pF
Battery	Li-Ion, Rechargeable
Autonomy (typ.)	8 h
Communication	Bluetooth
Physical Dimensions	141 mm × 81 mm × 32 mm
Weight	350 g

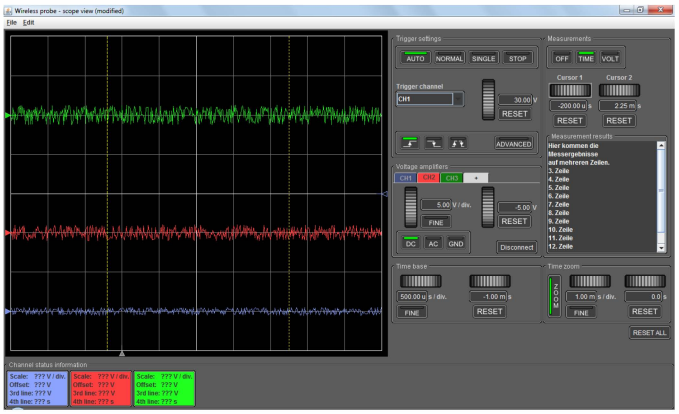

Fig. 9: Graphical User Interface prototype of the wireless oscilloscope implemented in Java. User settings: trigger mode, channel, level and slope; vertical settings like Volts/div, offset, signal coupling; horizontal settings such as Time/div, trigger position; horizontal zoom function; cursors. Outputs: display of waveforms and settings for each channel; cursors; split screen view in zoom-mode; export / import of measurement data and settings.

By means of the implemented wireless oscilloscope prototype, an evaluation of this system and a comparison to commercial isolated measurement systems will be made in the next section.

IV. Experimental Verification

In the following, the performance of the implemented wireless oscilloscope is analysed and compared to commercial isolated measurement systems.

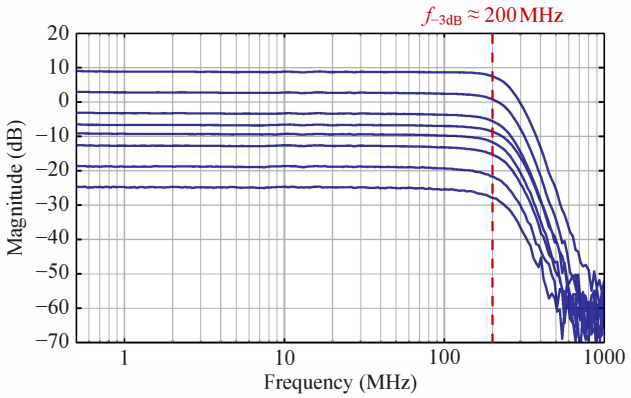

Fig. 10: Measured small-signal frequency characteristic of the wireless scope's analog frontend (from input voltage v_{IN} to the voltage at the A/D-converter v_{ADC}, cf. Fig. 8, for different input attenuations [17].

A. Analog Bandwidth

One of the key performance indicators of a measurement system is the analog bandwidth f_{-3dB}, which basically specifies at which upper frequency the measurement signal is attenuated from nominal gain by $-3\,dB$. The analog bandwidth of the wireless scope is determined by the channels analog frontend, cf. Fig. 8, i.e. by the transfer function from the input voltage v_{IN} to the voltage at the A/D-converter v_{ADC}.

Fig. 10 shows the measurements of this transfer function for the different input attenuations carried out by a network analyser (HP 4396A + HP 85046A). It can be summarized, that the frequency characteristic of the analog frontend is flat, i.e. the deviations are below $1\,dB$ up to $100\,MHz$, and the analog bandwidth is about $200\,MHz$ for all different input attenuations.

In addition to the analog frontend also the A/D-conversion influences the maximum overall bandwidth of the system, whereby the sample rate limits the signal rise time. If the typical rule of thumb relation between rise time t_{rise} and bandwidth f_{-3dB},

$$t_{rise} \approx \frac{0.35}{f_{-3dB}}, \tag{5}$$

is considered, reasonably a maximum bandwidth of ca. $140\,MHz$ can be obtained with the sampling rate of $400\,MS/s$. With some safety margin, an analog bandwidth of DC – $100\,MHz$ is thus specified for the wireless oscilloscope.

B. Common Mode Rejection

In order to achieve accurate measurements on floating potential, the isolated voltage and / or current measurement system must provide a very high Common Mode Rejection Ratio,

$$CMRR_{dB} = 20\log_{10}\left(\frac{A_{DM}}{A_{CM}}\right) = 20\log_{10}\left(\frac{v_{CM}}{v_M}\right), \tag{6}$$

which can also be calculated out of the measurement system's output voltage v_M at shorted probe leads on floating common mode voltage v_{CM}.

In the following, the CM rejection of the wireless scope and three different state of the art differential probes have been measured at $f = 200\,kHz$ in order to evaluate and compare these systems. Fig. 11 shows the measurement setup, which was used for that purpose, and the measured waveforms thereby. The corresponding CMRR values have been calculated according to (6) and are listed in Table II.

It can be stated, that the wireless scope provides an approximately 10- to 100-times higher common mode rejection compared to the

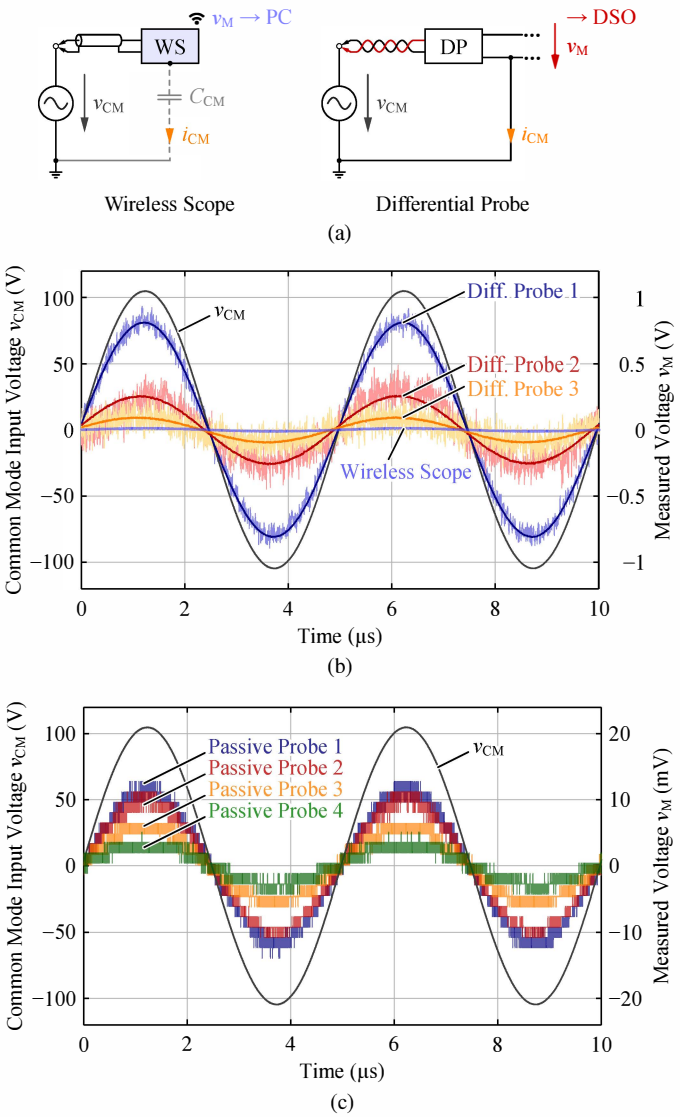

Fig. 11: Measurement of the common mode rejection of the wireless scope prototype and three commercial differential probes by means of shorted probe leads connected to a $f = 200\,kHz$ floating reference voltage v_{CM}. (a) Test setup; Measured voltages v_M by (b) the differential probes (solid: average over 1000 measurements) and the wireless scope and (c) the wireless scope with different 1:10 passive probes.

Measurement System	CMRR
Differential Probe 1, 25 MHz	42 dB
Differential Probe 2, 100 MHz	54 dB
Differential Probe 3, 100 MHz	61 dB
Wireless Scope + 1:10 Passive Probe 1	79 dB
Wireless Scope + 1:10 Passive Probe 2	80 dB
Wireless Scope + 1:10 Passive Probe 3	85 dB
Wireless Scope + 1:10 Passive Probe 4	90 dB
Wireless Scope + 1:1 Passive Probe	100 dB

TABLE II: Common mode rejection ratios at 200 kHz.

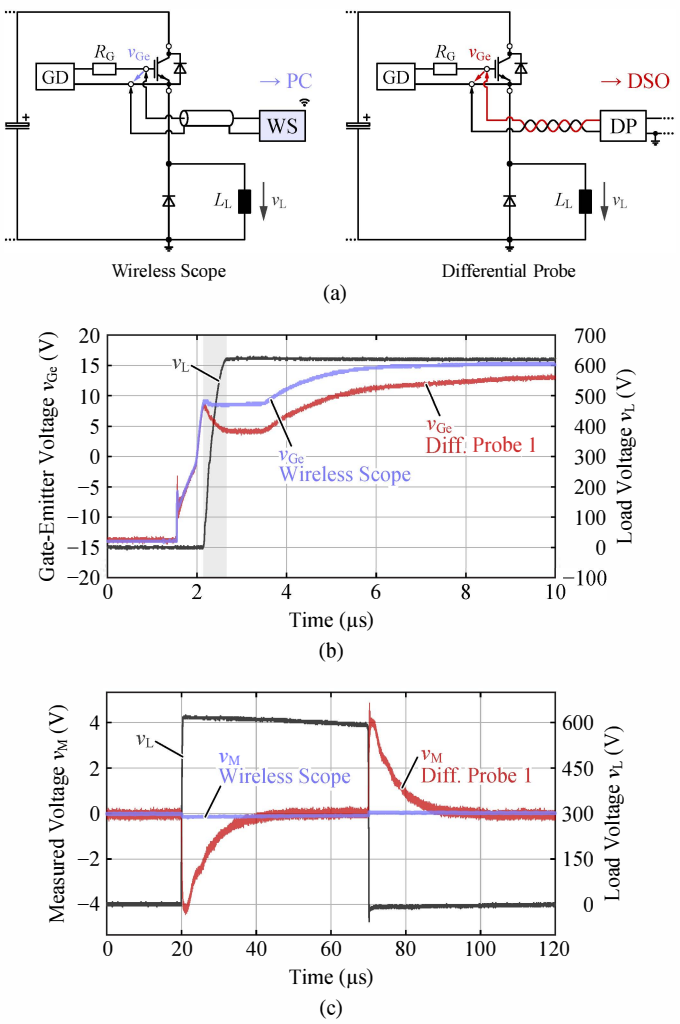

Fig. 12: Measurement of an IGBT's gate voltage v_{Ge} floating on the reference potential v_L by the wireless scope and a commercial differential probe. (a) Test setup; (b) Measured Gate-emitter voltages v_{Ge} and load voltage v_L; (c) Measured voltages v_M for shorted probe leads connected to the load voltage.

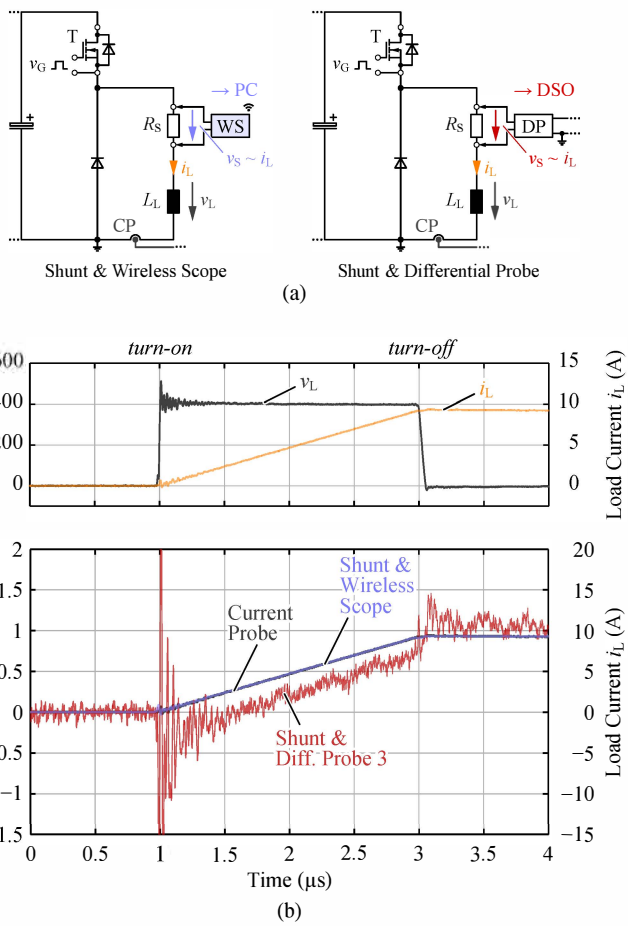

Fig. 13: Load current i_L measurement by means of a floating coaxial shunt $R_S \approx 0.1\,\Omega$) and the wireless scope or a differential probe. (a) Measurement setup; (b) Measured load voltage v_L and load currents i_L of both systems. As a reference, i_L was measured with a 50 MHz current compensated clamp-on probe on the non-floating side of the load.

best differential probe tested. The effective CMRR of the wireless scope finally depends on the utilized passive probe, whose parasitic capacitances, which depend on the mechanical setup, have an impact on the CM current i_{CM} and thus the CMRR.

In the following, the benefits of the wireless scope's superior CM rejection will be illustrated.

C. Voltage Measurement on Floating Potential

A very typical application, which demands an isolated voltage measurement system, is the gate voltage measurement of a floating power semiconductor. In order to test and compare the wireless scope to a differential probe, the Gate-emitter voltage of a floating high-side IGBT was measured by both systems. Fig. 12 (a, b) shows the related test setup and the corresponding measurements of the floating emitter / load voltage v_L as well as the IGBT's Gate-emitter voltage v_{Ge}.

Both systems measure the gate voltage appropriately, as long as the load voltage stays constant. During the CM voltage step of v_L, due to the high CMRR, the wireless scope measures the Miller plateau of v_{Ge} flat as expected. In contrast, a significant error appears at the measurement of the differential probe, i.e. the gate voltage drops unexpectedly by ca. 4 V. In addition, this error is not only apparent during the CM transients but decays with slow dynamics.

In order to examine this CM error separately, in Fig. 12 (c) the measured voltages v_M for shorted probe leads (0 V differential input voltage) connected to the floating load voltage are shown. The CM error of the wireless scope is considerably small compared to the differential probe. There, the error is injected during the CM step and it only decays exponentially with the time constant $\tau_{CM,DP1} \approx 7\,\mu s$. Another advantage of the wireless scope is the significantly lower noise level compared to the differential probe.

D. Current Measurement on Floating Potential

In addition to voltages also currents need to be measured with respect to floating potentials. Since an input channel of the wireless scope is inherently isolated, it's basically possible to utilize e.g. a non-isolated coaxial shunt on floating potential as an isolated current sensor. The performance of such an arrangement, cf. Fig. 13 (a), was experimentally investigated and compared to combining the shunt with a differential probe in Fig. 13 (b).

The load current waveform of the wireless scope is identical to the reference measurement by the current compensated clamp-on probe. In contrast, the waveform of the differential probe shows a strong

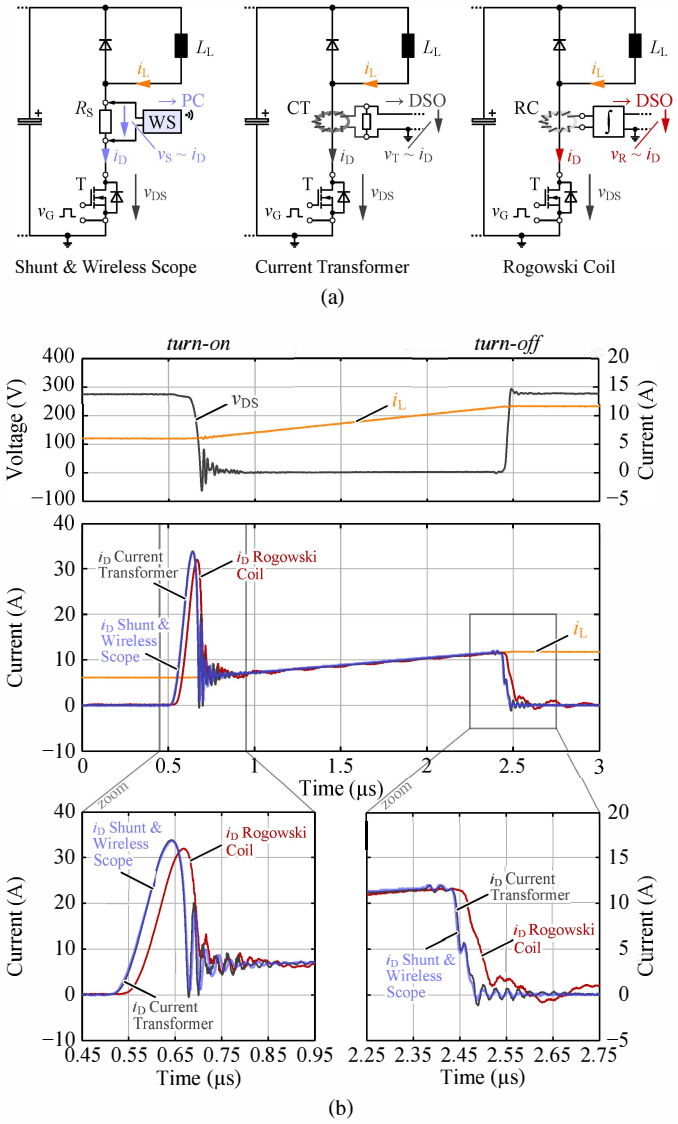

Fig. 14: Low-side Drain current i_D measurement at hard switching by means of the wireless scope and a 0.1 Ω coaxial shunt, a 100 MHz passive current transformer and an active 30 MHz Rogowski coil. (a) Test setup; Measured load voltage v_L and Drain currents i_D of all systems.

ringing and a deviation due to the transient CM voltage step, and also exhibits a comparably large noise level. As a result, in contrast to the differential probe, the wireless scope finally enables to employ low-ohmic coaxial shunt resistors as an isolated current sensor with low CM sensitivity and low noise.

In a next step, the bandwidth of this measurement concept is further investigated by a measurement of a floating MOSFET Drain current exhibiting high frequency components at hard switching, cf. Fig. 14. In addition, this measurement is compared to other isolated current measurement concepts, such as a passive current transformer and an active Rogowski coil.

The 30 MHz bandwidth of the Rogowski Coil is not high enough to measure the high frequency ringing after the diode reverse recovery snap-off. In addition, the signal of the Rogowski coil is delayed and a ringing is excited after the CM voltage step. Between the measurements of the current transformer and the wireless scope with shunt basically no difference can be visualized. The main benefits of the wireless scope with shunt over the current transformer is the high voltage isolation and the possibility of measuring DC currents.

V. Summary and Outlook

The measurement of current and voltage by means of a wireless oscilloscope with high-isolated input channels was identified to have clear advantages with respect to state of the art isolated voltage and current measurement concepts. The implementation details of the key components in the wireless oscilloscope, the isolated measurement channels, and the respective user interface of the system were shown.

The experimental evaluation of the wireless scope confirmed the extraordinary performance of this measurement concept. The isolated channel offers an analog bandwidth of 100 MHz at basically unlimited voltage isolation and exhibits a 10- to 100-times higher common mode rejection and a significantly higher signal-to-noise ratio than state of the art differential probes. In addition, the isolated input channels enable employing non-isolated / high-bandwidth sensors, e.g. shunt resistors, on floating potential, thus opening new possibilities in measurement and testing of electric circuitry.

References

[1] A. Nara, "A measurement of the gate-emitter voltage waveform of IGBT in a motor driver circuit," in *Proc. of the 10th IEEE Instrumentation and Measurement Technology Conf. (IMTC)*, Hamamatsu, Japan, May 1994, pp. 623–626.

[2] W. H. Siew, Y. Wang, and M. Faheem, "Digital wireless electromagnetic interference (EMI) data acquisition system," in *Proc. of the Int. Symp. on Electromagnetic Compatibility (EMC)*, vol. 2, Aug. 2005, pp. 342–345.

[3] Y. Lobsiger, D. Bortis, H. Ertl, and J. W. Kolar, "100 MS/s 10-25 MHz wireless voltage probe," in *Proc. of the Power Conversion and Intelligent Motion Conf. (PCIM Europe)*, Nuremberg, Germany, May 2011, pp. 627–633.

[4] F. Costa, E. Labouree, F. Forest, and C. Gautier, "Wide bandwidth, large AC current probe for power electronics and EMI measurements," *IEEE Trans. Ind. Electron.*, vol. 44, no. 4, pp. 502–511, Aug. 1997.

[5] S. Ziegler, R. C. Woodward, H. H.-C. Iu, and L. J. Borle, "Current Sensing Techniques: A Review," *IEEE Sensors Journal*, vol. 9, no. 4, pp. 354–376, Apr. 2009.

[6] *Isolated current and voltage transducers, 3rd ed.*, LEM Components, Plan-les-Ouates, Switzerland, 2004.

[7] P. Ripka, "Review of Fluxgate Sensors," *Sensors and Actuators A: Physical*, vol. 33, no. 4, pp. 129–141, 1992.

[8] W. F. Ray and C. R. Hewson, "High performance Rogowski current transducers," in *Proc. of the Ind. Appl. Conf.*, vol. 5, Rome, Italy, Oct. 8-12, 2000, pp. 3083–3090.

[9] Lecroy, 2014. [Online]. Available: teledynelecroy.com

[10] Tektronix, 2014. [Online]. Available: www.tek.com

[11] Agilent, 2014. [Online]. Available: www.home.agilent.com

[12] Yokogawa, 2014. [Online]. Available: www.yokogawa.com

[13] Rhode & Schwarz, 2014. [Online]. Available: www.rohde-schwarz.com

[14] Inventronik, 2014. [Online]. Available: www.inventronik.de

[15] OMICRON Lab, 2014. [Online]. Available: www.omicron-lab.com

[16] Power Electronic Measurement, 2014. [Online]. Available: www.pemuk.com

[17] O. Knecht, "Entwicklung eines Tastkopfs zur potentialfreien Spannungsmessung (in German)," Master's thesis, Power Electronic Systems Laboratory, ETH Zurich, Mar. 2013.